IEEE Transactions on Quantum Engineering

Received 26 March 2024; revised 18 July 2024; accepted 29 July 2024; date of publication 6 August 2024; date of current version 29 August 2024.

Digital Object Identifier 10.1109/TQE.2024.3439135

Noise Robustness of Quantum Relaxation for Combinatorial Optimization

KENTARO TAMURA[1], YOHICHI SUZUKI[2], RUDY RAYMOND[2,3,4], HIROSHI C. WATANABE[2,5], YUKI SATO[2,6], RUHO KONDO[2,6], MICHIHIKO SUGAWARA[2], AND NAOKI YAMAMOTO[1,2]

[1]Department of Applied Physics and Physico-Informatics, Keio University, Yokohama 223-8522, Japan
[2]Quantum Computing Center, Keio University, Yokohama 223-8522, Japan
[3]IBM Quantum, IBM Japan, Tokyo 103-8510, Japan
[4]Department of Computer Science, University of Tokyo, Tokyo 113-0033, Japan
[5]Department of Chemistry, Graduate School of Science, Kyushu University, Fukuoka 819-0395, Japan
[6]Toyota Central R&D Labs., Inc., Aichi 480-1192, Japan

Corresponding author: Kentaro Tamura (e-mail: cicero@keio.jp).

The work of Naoki Yamamoto was supported by the MEXT Quantum Leap Flagship Program under Grant JPMXS0118067285 and Grant JPMXS0120319794.

ABSTRACT Relaxation is a common way for dealing with combinatorial optimization problems. Quantum random-access optimization (QRAO) is a quantum-relaxation-based optimizer that uses fewer qubits than the number of bits in the original problem by encoding multiple variables per qubit using quantum random-access code (QRAC). Reducing the number of qubits will alleviate physical noise (typically, decoherence), and as a result, the quality of the binary solution of QRAO may be robust against noise, which is, however, unknown. In this article, we numerically demonstrate that the mean approximation ratio of the (3, 1)-QRAC Hamiltonian, i.e., the Hamiltonian utilizing the encoding of three bits into one qubit by QRAC, is less affected by noise compared with the conventional Ising Hamiltonian used in the quantum annealer and the quantum approximate optimization algorithm. Based on this observation, we discuss a plausible mechanism behind the robustness of QRAO under depolarizing noise. Finally, we assess the number of shots required to estimate the values of binary variables correctly under depolarizing noise and show that the (3, 1)-QRAC Hamiltonian requires less shots to achieve the same accuracy compared with the Ising Hamiltonian.

INDEX TERMS Combinatorial optimization, depolarizing noise, quantum random-access code (QRAC), quantum relaxation.

I. INTRODUCTION

Combinatorial optimization is the task of finding an optimum value of a function defined on some finite domain [1]. The task has a wide range of applications ranging from industry [2], [3] to finance [4], [5]. Quantum-relaxation-based optimizers, such as variational quantum eigensolver (VQE) [6] and quantum approximate optimization algorithm (QAOA) [7], [8], have been thoroughly investigated, but they share a common scalability problem [9] when executed on a real quantum device. That is, on real quantum devices, the number of sequential gate operations while sustaining a coherent quantum state is restricted by noisy operations, such as decoherence and the limited number of qubits [10]. One way to recover scalability is to reduce the number of qubits in a circuit, for example, by cutting a large circuit into smaller subcircuits with fewer qubits and less sequential gate operations [11]. In quantum algorithms for optimization, the number of qubits employed is determined by the encoding of a problem, i.e., how to map classical variables onto qubits. Various encodings have been proposed to achieve a more efficient encoding [12], [13]. Among them is the quantum random-access optimization (QRAO) algorithm proposed by Fuller et al. [14], which utilizes quantum random-access code (QRAC) [15] to encode multiple binary variables per qubit, thereby reducing the number of qubits required for problem mapping.

QRAC was first proposed in the context of communication in order to encode as many classical bits per qubit as possible. The central idea was to exceed the Holevo bound [16] that forbids encoding m bits into less number of qubits without information loss by allowing a possibility of decoding the wrong bit. The encoding of m binary variables on n qubits with decoding probability p is denoted as (m, n, p)-QRAC [15]. There are (2,1,0.85)-QRAC,

(3,1,0.78)-QRAC [15], [17], and several other constructions of $(m, 2, p > 1/2)$-QRAC [18], [19], [20]. For simplicity, the probability $p > 1/2$ in (m, n, p)-QRAC is omitted and written as (m, n)-QRAC from now on.

QRAO [14], [21], [22], [23] differs from algorithms, such as QAOA, in that it involves a process called the quantum state rounding. Quantum state rounding is the mapping of the candidate quantum state (with continuous degree of freedom) obtained by a quantum optimizer, such as VQE, onto a binary solution (with discrete degree of freedom). Because a candidate state perturbed by noise may still be mapped to the same binary solution, we have the intuition that the solution of QRAO may be robust to noise. In this article, therefore, we investigate the effect of noise on the quality of the binary solution obtained by QRAO in the following manner.

1) We encode the same combinatorial optimization problems onto two Hamiltonians: the QRAC Hamiltonian and the Ising Hamiltonian.
2) We then use the same ansatz and optimizer for the VQE to obtain the candidate states for both the cases of Hamiltonian. We do not use the QAOA approach because it is not commonly used in the context of QRAO; instead, the VQE ansatz is typically employed. In our study, we use the VQE ansatz for the Ising Hamiltonian because our objective is to explore the properties of QRAO by comparing the QRAC Hamiltonian with the Ising Hamiltonian.
3) Finally, we compare the binary solutions using the approximation ratio, which is the ratio between the value of cost function of the binary solution at hand and the optimal binary solution. Note that, while the effect of noise on QRAC in its original context has been reported [24], the effect of noise on QRAC in the context of optimization is unknown.

Here is the summary of the result. We demonstrate through simulation using a noiseless device that as the problem size increases, the mean approximation ratio resulting from the (3, 1)-QRAC Hamiltonian exceeds the mean approximation ratio resulting from the Ising Hamiltonian. The simulation results under fake noise [25] show that the mean approximation ratio obtained by the (3, 1)-QRAC Hamiltonian is more robust to noise than in the Ising Hamiltonian case. We provide a theoretical explanation for the effect of noise on the mean approximation ratio of QRAO by assuming depolarizing noise. Finally, we derive the order of shots required in Pauli rounding to achieve a given successful decoding probability under depolarizing noise.

II. PRELIMINARY

A. MAXIMUM CUT (MAXCUT) PROBLEM

In this article, we deal with the unweighted MaxCut problem. The MaxCut problem is an NP-hard combinatorial problem involving undirected graphs [26]. Given an undirected graph G with $|V|$ nodes labeled v_i and $|E|$ edges labeled $e_{i,j}$, the objective of the MaxCut problem is to find a configuration $m_i \in \{0, 1\}$ that maximizes the cost function

$$\max_{m\in\{0,1\}^{|V|}} \text{cut}(m) \tag{1}$$

where

$$\text{cut}(m) := \frac{1}{2}\sum_{e_{i,j}\in E}(1-(-1)^{m_i+m_j}).$$

For example, one of the optimal solutions to the MaxCut problem for a four-node graph is shown in Fig. 1(a), where three out of three edges are included in the cut.

The solution accuracy is evaluated by the approximation ratio defined by the ratio between the obtained cut value $\text{cut}(m)$ and the optimal cut value $\text{cut}(m^*)$. The approximation ratio $\gamma = \text{cut}(m)/\text{cut}(m^*)$ is a real number ranging from 0 to 1. For example, the approximation ratio of the output in Fig. 1(a) is $\gamma = 3/3 = 1.0$.

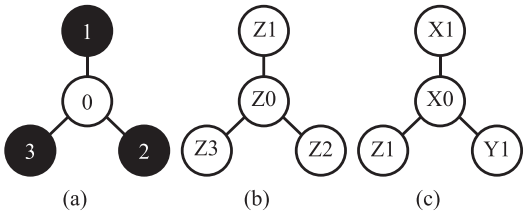

FIGURE 1. (a) One of the optimal configurations of the MaxCut problem for a four-node graph. (b) Example of a Ising encoding for a four-node graph using four qubits, where *Zi* corresponds to the Pauli matrix *Z* on the qubit index *i*. (c) Example of a (3, 1)-QRAC encoding for a four-node graph using two qubits, where *Pi* corresponds to the Pauli matrix $P \in \{X, Y, Z\}$ on the qubit index *i*.

B. QUANTUM RANDOM-ACCESS OPTIMIZATION

QRAO [14] is a relaxation-based optimization algorithm that uses QRAC to solve binary optimization problems. The use of QRAC enables us to save the number of qubits to one-third as many qubits as the number of binary variables (bits). Decoding the binary solution from the qubits requires a specific measurement procedure rather than a simple measurement in the computational basis. QRAO consists of three steps: encoding, optimization, and rounding. In encoding, we construct the QRAC Hamiltonian, which encodes the binary optimization problem in a relaxed manner. In optimization, the VQE is carried out based on the QRAC Hamiltonian. The binary solution is then estimated from the resulting quantum state through a measurement process termed quantum state rounding. In this section, we overview each step of the algorithm with the MaxCut problem as an example.

1) ENCODING

In this article, we define *encoding* as the embedding of classical bits into qubits. In the conventional Ising-type formulation [7], the classical bit 0 is encoded to $|0\rangle$ and 1 to $|1\rangle$, which can be viewed as the ith node of the graph is assigned to the Pauli matrix Z_i supported by the ith qubit. Hence, the score

IEEE Transactions on Quantum Engineering

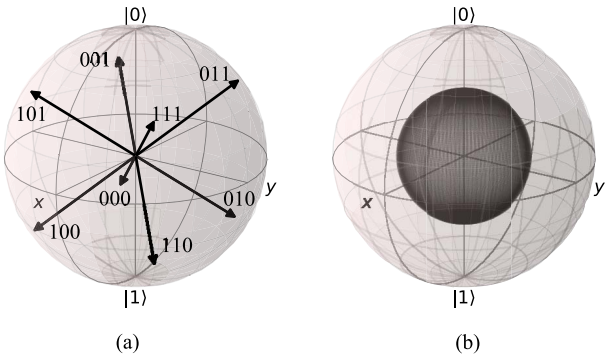

FIGURE 2. (a) Bloch sphere representation of (3,1)-QRAC. (b) Bloch sphere representation of the depolarizing channel with error probability 0.5.

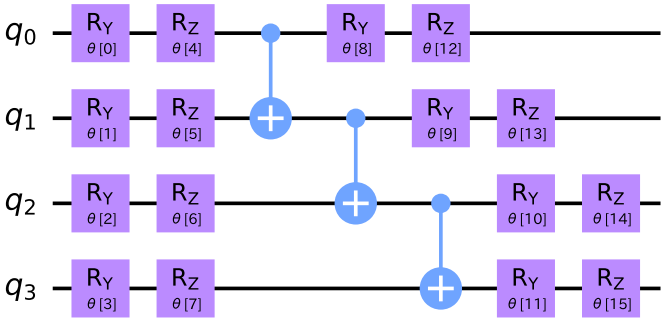

FIGURE 3. Four-qubit single-layer hardware-efficient ansatz with linear entanglement.

of $e_{i,j}$ is defined as $\frac{1}{2}(I - Z_iZ_j)$. As a result, the MaxCut problem of a graph G is equivalent to the maximization of the mean value of the following Ising Hamiltonian:

$$H_{\text{Ising}} = \frac{1}{2}\sum_{e_{i,j}\in E}(I - Z_iZ_j). \tag{2}$$

In the QRAC formulation, the classical bits (x_1, x_2, and x_3) are encoded to a single qubit as

$$f(x_1, x_2, x_3) = \frac{1}{2}\left(I + \frac{1}{\sqrt{3}}((-1)^{x_1}X + (-1)^{x_2}Y + (-1)^{x_3}Z)\right) \tag{3}$$

where X, Y, and Z are Pauli matrices, I is the identity matrix, and $x_1, x_2, x_3 \in \{0, 1\}$. The encoded states are plotted at the vertices of a cube in the Bloch sphere, as in Fig. 2(a). One can assign at most three nodes to each qubit with the constraint that adjacent nodes must be assigned to different qubits. The Hamiltonian is constructed as

$$H = \frac{1}{2}\sum_{e_{i,j}\in E}(I - 3P_iP_j) \tag{4}$$

where P_i corresponds to the Pauli matrix assigned to the ith node. For a candidate state $F(m)$ that is a product state of f, we have [14]

$$\text{Tr}(F(m)H) = \text{cut}(m).$$

Note that as H is a relaxed Hamiltonian, the expectation value may exceed the maximum cut value. The relation between the cut value and the (3, 1)-QRAC Hamiltonian is clarified in Section II-B3b. We expect that maximizing the expectation value of the candidate state with respect to the Hamiltonian results in a closer state to $F(m)$.

2) OPTIMIZATION

In the optimization step, the expectation value of the QRAC Hamiltonian is maximized by varying the quantum state via variational methods, such as VQE, QAOA, or other more recent ones [27], [28]. In the present study, we carry out the VQE with the hardware efficient [29] to obtain the candidate state. An example of the ansatz with four qubits is shown in Fig. 3. Although we are aware that there are various optimizers for parameterized quantum circuits (PQCs), including free-axis selection [30], and free-quaternion selection [31], [32], we consistently used the Nakanishi–Fujii–Todo (NFT) algorithm (also termed Rotosolve) [33], [34] for both the Ising and QRAC Hamiltonians.

3) QUANTUM STATE ROUNDING

The maximum-eigenvalue eigenstates of the Ising Hamiltonian directly correspond to the classical solution because the Ising Hamiltonian is diagonal in the computational basis. To obtain the classical solution, therefore, one needs only to apply measurement in the computational basis $\{|0\rangle, |1\rangle\}$. In contrast, the eigenstates of the (3, 1)-QRAC Hamiltonian are not necessarily diagonal in the computational basis; the obtained eigenstates are in entanglement and superposition in general. To obtain the classical solution, a procedure called quantum state rounding is required. QRAO has two methods of rounding: Pauli rounding and magic state rounding [14].

a) Pauli rounding

In Pauli rounding, the classical bits are decoded by estimating the expectation values of Pauli matrices as observables. Given a candidate state ρ, the classical bit is decoded by estimating the sign of the trace value $\text{Tr}(P_i\rho)$, where P_i denotes the Pauli matrix corresponding to the node i. If the trace value is positive, $+1$ is assigned, if negative, -1 is assigned, and if 0, a bit of 0 or 1 is assigned uniformly at random. For the case of example shown in Fig. 1(c), when the corresponding qubit index and the Pauli string for node 0 are 0 and X, respectively, $\text{Tr}[(X \otimes I)\rho]$ is used to decode the classical bit of node 0. Here, the Pauli matrix on the far left corresponds to the qubit with the smallest index.

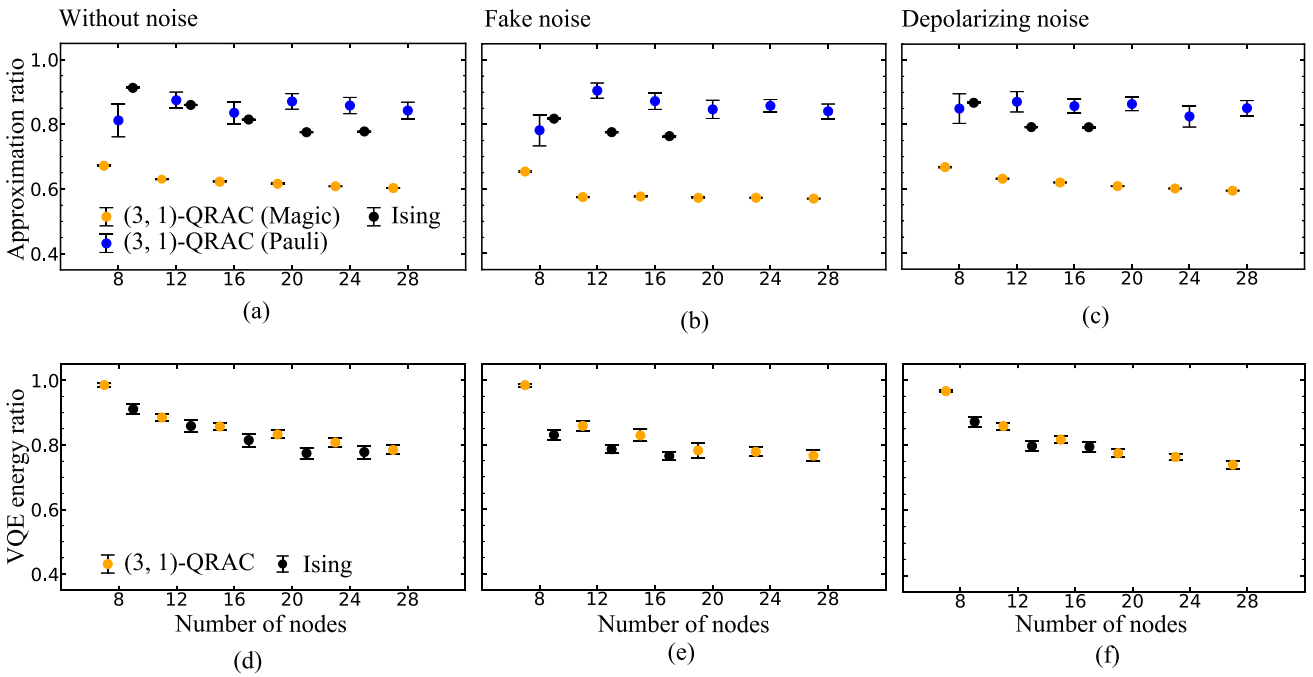

FIGURE 4. Quantum state rounding results of candidate states obtained via the VQE. The number of nodes on the *x*-axis corresponds to three plots positioned to the left, center, and right. The error bars denote the 95% confidence intervals. (a) Results under no noise. (b) Results of fake back-end FakeMumbaiV2 [25] provided by IBM. (c) Results under depolarizing noise with error probability 1% on the controlled-NOT gates. (d)–(f) Mean of the VQE energy ratio corresponding to the candidate states of (a)–(c), respectively, where orange refers to the QRAC Hamiltonian and black the Ising Hamiltonian. The VQE energy ratio for the QRAC Hamiltonian has been rescaled.

b) Magic state rounding

In magic state rounding, each qubit of the candidate state is measured along the following four bases uniformly at random:

$$\mu_1^{\pm} = \frac{1}{2}\left(I \pm \frac{1}{\sqrt{3}}(X+Y+Z)\right)$$
$$\mu_2^{\pm} = \frac{1}{2}\left(I \pm \frac{1}{\sqrt{3}}(X-Y-Z)\right)$$
$$\mu_3^{\pm} = \frac{1}{2}\left(I \pm \frac{1}{\sqrt{3}}(-X+Y-Z)\right)$$
$$\mu_4^{\pm} = \frac{1}{2}\left(I \pm \frac{1}{\sqrt{3}}(-X-Y+Z)\right).$$

This procedure is equivalent to mapping each qubit to one of the eight states shown in Fig. 2(a). A single iteration of magic state rounding involves measuring each qubit on the randomly assigned basis $\{\mu_i^+, \mu_i^-\}$, where $i \in [4]$. This is repeated for a number of times, and the solution with the highest approximation ratio becomes the final output. The lower bound for the expected approximation ratio for magic state rounding is known to be [14]

$$\mathbb{E}(\gamma) = \mathbb{E}\left[\frac{\mathrm{cut}(m)}{\mathrm{cut}(m^*)}\right] = \frac{\mathbb{E}\left[\mathrm{Tr}(\mathcal{M}^{\otimes n}(\rho)H)\right]}{\mathrm{Tr}(F(m^*)H)} \geq \frac{5}{9} \quad (5)$$

where $F(m^*)$ is a map that achieves $\mathrm{Tr}(F(m^*)H) = \mathrm{cut}(m^*)$, and m^* is the optimal configuration. Here, $\mathcal{M}^{\otimes n}(\rho)$ is defined as the n-qubit state resulting from a single shot of magic state rounding, which is a product state of the eight QRAC states shown in Fig. 2(a) in the case of (3, 1)-QRAC [14]. A recent study has revealed that the expected value of the (3,1)-QRAC Hamiltonian has the relation $\mathrm{Tr}(H\rho) = 9\mathbb{E}(\mathrm{Tr}(\mathcal{M}^{\otimes n}(\rho)H)) - 4|E|$, where $\mathbb{E}(\mathrm{Tr}(\mathcal{M}^{\otimes n}(\rho)H))$ represents the expected cut value via magic state rounding [23].

III. RESULTS AND DISCUSSION

Our main result is shown in Fig. 4. We will, henceforth, refer to the (3, 1)-QRAC Hamiltonian as the QRAC Hamiltonian. The approximation ratio corresponding to the QRAC Hamiltonian is obtained by Pauli rounding unless specified otherwise.

A. SIMULATION RESULTS OF QRAO UNDER NOISE

To examine the effect of noise on the approximation ratio of QRAO, we solved the MaxCut problem for random three-regular graphs with the QRAC Hamiltonian and the Ising Hamiltonian using candidate states obtained by using the following devices:

1) statevector simulator without noise;
2) statevector simulator with fake noise;
3) statevector simulator with depolarizing noise with error probability 1% on all the controlled-NOT gates.

IEEE Transactions on Quantum Engineering

The VQE was executed with 1024 shots for each Pauli term to estimate the energy expectation value. Fake noise refers to a noise model that mimics the behavior of a real device by combining the single-qubit depolarizing error, single-qubit thermal relaxation error, two-qubit depolarizing error, and the single-qubit readout error, whose parameters are tuned based on real system snapshots [25]. For both the types of Hamiltonian, the candidate states were prepared via the VQE with three layers of the hardware efficient ansatz shown in Fig. 3(b) and two parameter sweeps with the NFT algorithm. Here, two parameter sweeps refer to the process of updating each parameter in the parameterized circuit (ansatz) twice via the NFT optimizer. We employed the linear entanglement ansatz, in which case the controlled-NOT gate depth is $n-1$ for n qubits per layer. Noisy simulations for graphs with 20 nodes or more via the Ising Hamiltonian could not be executed in a reasonable amount of time. This constraint arises from the fact that we performed noisy simulations. Noisy simulations can be done by either the density matrix simulator or the statevector simulator. The former uses $2^n \times 2^n$ matrices for n-qubit simulations, and the latter requires extensive sampling to simulate the effect of noise. The mean approximation ratio $\overline{\gamma}_{|V|}$ for 50 $|V|$-node graphs for the Ising Hamiltonian and the QRAC Hamiltonian (magic state rounding) is defined by

$$\overline{\gamma}_{|V|} = \frac{1}{25000}\sum_{j=1}^{50}\sum_{k=1}^{500}(\gamma_{|V|_j})_k$$

where $|V|_j$ denotes the number of nodes of the jth graph ranging from $j=1$ to 50, and k denotes the kth measurement result. The mean approximation ratio $\overline{\gamma}_{|V|}$ for 50 $|V|$-node graphs of the QRAC Hamiltonian via Pauli rounding is defined by

$$\overline{\gamma}_{|V|} = \frac{1}{50}\sum_{j=1}^{50}\gamma_{|V|_j}.$$

The mean approximation ratios obtained by the respective devices are shown in Fig. 4(a)–(c). The error bars of the mean approximation ratios represent the 95% confidence intervals defined by

$$\left(\overline{\gamma}_{|V|} - 1.96\frac{\sigma_{\overline{\gamma}_{|V|}}}{\sqrt{25000}}, \overline{\gamma}_{|V|} + 1.96\frac{\sigma_{\overline{\gamma}_{|V|}}}{\sqrt{25000}}\right)$$

for the Ising Hamiltonian and the QRAC Hamiltonian via magic state rounding, where

$$\sigma_{\overline{\gamma}_{|V|}} = \sqrt{\frac{1}{25000}\sum_{j=1}^{50}\sum_{k=1}^{500}\left((\gamma_{|V|_j})_k - \overline{\gamma}_{|V|}\right)^2}$$

and

$$\left(\overline{\gamma}_{|V|} - 1.96\frac{\sigma_{\overline{\gamma}_{|V|}}}{\sqrt{50}}, \overline{\gamma}_{|V|} + 1.96\frac{\sigma_{\overline{\gamma}_{|V|}}}{\sqrt{50}}\right)$$

for the QRAC Hamiltonian via Pauli rounding, where

$$\sigma_{\overline{\gamma}_{|V|}} = \sqrt{\frac{1}{50}\sum_{j=1}^{50}\left(\gamma_{|V|_j} - \overline{\gamma}_{|V|}\right)^2}.$$

The ratio between the achieved energy of the candidate state and the maximum eigenvalue of the Hamiltonian is shown in Fig. 4(d)–(f), along with 95% confidence intervals. The VQE energy ratio for 50 $|V|$-node three-regular graphs is defined by

$$\overline{E}(|V|) = \frac{1}{50}\sum_{j=1}^{50}\tilde{E}_j$$

where

$$\tilde{E}_j := \frac{E_j - E_{j,\max}}{E_{j,\max} - E_{j,\min}}$$

and the 95% confidence interval is defined by

$$\left(\overline{E}(|V|) - \frac{1.96}{\sqrt{50}}\sqrt{\sum_{j=1}^{50}\left(\tilde{E}_j - \overline{E}(|V|)\right)^2}\right.$$
$$\left.\overline{E}(|V|) + \frac{1.96}{\sqrt{50}}\sqrt{\sum_{j=1}^{50}\left(\tilde{E}_j - \overline{E}(|V|)\right)^2}\right)$$

where E_j is the VQE energy expectation value for the jth graph, and $E_{j,\min}$ and $E_{j,\max}$ are the minimum and maximum eigenvalues of the jth graph, respectively. Note that the VQE energy E_j for the QRAC Hamiltonian has been rescaled by $(E_j - E_{j,\min})/(E_{j,\max} - E_{j,\min})$. For each number of nodes, 50 random three-regular graphs were solved.

Fig. 4(a) shows the simulation results of the statevector simulator without noise. It shows that as the problem size characterized by the number of nodes increases, the mean approximation ratio of the QRAC Hamiltonian exceeds that of the Ising Hamiltonian. The mean approximation ratio of the Ising Hamiltonian shows a significant decline outside the 95% confidence interval from 8 to 20 nodes, while the mean approximation ratio of the QRAC Hamiltonian does not. From Fig. 4(d), we observe that there is no significant difference in the VQE energy ratio between the candidate states of the QRAC Hamiltonian and the Ising Hamiltonian at 20 nodes or more. However, the mean approximation of the QRAC Hamiltonian at 20 nodes is significantly higher than that of the Ising Hamiltonian. This indicates that the QRAC tends to yield a higher approximation ratio with respect to the VQE energy ratio.

Fig. 4(b) shows the mean approximation ratios obtained under fake noise. By comparing Fig. 4(a) and 4(b), we find that the mean approximation ratio of the Ising Hamiltonian shows a significant decline when subjected to noise, while the mean approximation ratio of the QRAC Hamiltonian does not. This implies that the mean approximation ratio of the QRAC Hamiltonian via Pauli rounding is robust to noise compared to the Ising Hamiltonian. Furthermore, the mean

approximation ratios of the QRAC Hamiltonian are higher than those of the Ising Hamiltonian with 12 and 16 nodes.

Fig. 4(c) shows the mean approximation ratio with the candidate states obtained under depolarizing noise with error probability 1% on the controlled-NOT gate. By comparing Fig. 4(a) and 4(c), we find that the mean approximation ratio of the QRAC Hamiltonian is robust to depolarizing noise as well. The simulation results under depolarizing noise capture the noise robustness of QRAO. We, therefore, explain the noise robustness of QRAO under the assumption of depolarizing noise in Section III-B.

B. QRAO UNDER DEPOLARIZING NOISE

Depolarizing noise is where an n-qubit quantum state ρ is mapped onto a linear combination of the unaffected state ρ and the completely mixed state $I/2^n$. The noise model has a parameter $p \in [0, 1]$, which can be interpreted as the probability that the state ρ remains unaffected by depolarizing noise. The state after a single application of depolarizing noise can be denoted as

$$\mathcal{D}_p(\rho) = p\rho + (1-p)\frac{I}{2^n}. \tag{6}$$

Depolarizing noise has the effect of "shrinking" the Bloch sphere, as shown in Fig. 2(b). After N applications of depolarizing noise, the resulting state becomes [35]

$$\mathcal{D}_p^N(\rho) = p^N\rho + \left(1-p^N\right)\frac{I}{2^n} \tag{7}$$

where N refers to the depth of noisy controlled-NOT gates in the circuit.

The robustness of the approximation ratio of Pauli rounding can be explained by the fact that the sign of the trace values is unaffected by depolarizing noise

$$\begin{aligned}\mathrm{Tr}(P_j\mathcal{D}_p^N(\rho)) &= \mathrm{Tr}\left[P_j\left(p^N\rho + (1-p^N)\frac{I}{2^n}\right)\right]\\ &= p^N\mathrm{Tr}[P_j\rho] + (1-p^N)\mathrm{Tr}\left[P_j\frac{I}{2^n}\right]\\ &= p^N\mathrm{Tr}[P_j\rho]\end{aligned} \tag{8}$$

where P_j is the Pauli matrix corresponding to the jth node, N is the number of depolarizing noise applications, n is the number of qubits of ρ, and ρ is the candidate state of the Hamiltonian. While the sign remains unchanged, the absolute trace values decrease under depolarizing noise, causing the number of shots required to correctly estimate their sign to increase. Suppose that $|V|$ Pauli matrices are assigned to a $|V|$-node graph. To estimate the sign of the trace value corresponding to each node with error probability at most δ, the minimum number of shots S is derived in the Appendix as

$$S \geq \frac{\ln(1/\delta)}{2\varepsilon^2}$$

and the order of shots as

$$\mathcal{O}\left(\frac{\ln(|V|)}{\varepsilon^2}\right).$$

Here, $\varepsilon > 0$ is defined by $\Pr(X_{ij} = 1) = 1/2 + \varepsilon$, where X_{ij} denotes the measurement result of 0 or 1 corresponding to the ith shot with respect to the Pauli matrix P_j assigned to the jth node. For $|V|$ Pauli matrices, the order of shots becomes

$$\mathcal{O}\left(\frac{|V|\ln(|V|)}{\varepsilon^2}\right). \tag{9}$$

As seen in (9), the order of shots grows quadratically with the decrease of ε. Under depolarizing noise, ε has the relation

$$\varepsilon = -p^N\mathrm{Tr}(P_j\rho)/2.$$

The minimum number of shots required under depolarizing noise can, thus, be written as

$$S \geq \frac{2\ln(1/\delta)}{p^{2N}\mathrm{Tr}(P_j\rho)^2}.$$

The inequality demonstrates the relationship between the number of qubits used and the minimum number of shots necessary to estimate $\mathrm{Tr}(P_j\rho)$ under depolarizing noise. Since the inequality can be applied to both the QRAC and Ising Hamiltonians, it also indicates that the QRAC Hamiltonian requires fewer shots than the Ising Hamiltonian under depolarizing noise. The number of shots required to correctly estimate all the trace values correctly grows exponentially with the number of depolarizing noise applications N and the number of nodes $|V|$, assuming that the QRAC Hamiltonian achieves the maximum compression rate where a $|V|$-node graph is encoded on one-third qubits, and that the candidate state is obtained via an ansatz with l linear entanglement layers whose controlled-NOT gates are under depolarizing noise. This results in $N = N_{\mathrm{CNOT}} = l|V|$ depolarizing noise applications, where N_{CNOT} denotes the number of controlled-NOT gates in the l-layered ansatz. The ratio of the minimum number of shots required for the QRAC Hamiltonian to the Ising Hamiltonian is then given by $p^{\frac{4}{3}l|V|}$, which indicates that estimating the correct configuration of all the nodes with the same level of accuracy requires more shots with the Ising Hamiltonian than with the QRAC Hamiltonian.

The effect of depolarizing noise on the expected approximation ratio of magic state rounding is as follows. Let ρ_1 and ρ_3 be density matrices corresponding to the Ising Hamiltonian H_1 and the QRAC Hamiltonian H_3 that satisfy $\mathrm{Tr}(H_1\rho_1) = \mathrm{cut}(m^*)$ and $\mathrm{Tr}(H_3\rho_3) \geq \mathrm{cut}(m^*)$, respectively. Without noise, the expected approximation ratio for ρ_1 is given by

$$\mathbb{E}(\gamma_1) = \frac{\mathrm{Tr}(H\rho_1)}{\mathrm{cut}(m^*)} = 1 \tag{10}$$

whereas the expected approximation ratio for ρ_3 via magic state rounding is given by

$$\mathbb{E}(\gamma_3) = \frac{\mathbb{E}\left[\mathrm{Tr}\left\{\mathcal{M}^{\otimes n_3}(\rho_3)H\right\}\right]}{\mathrm{cut}(m*)} \geq \frac{5}{9} \tag{11}$$

IEEE Transactions on Quantum Engineering

where n_3 represents the number of qubits of ρ_3. Now, let us consider parameterized circuits that output ρ_1 and ρ_3. We approximate the maximum-eigenvalue eigenstates by the VQE under depolarizing noise by assuming that the parameterized circuits contain N operations under the influence of depolarizing noise. The circuits that, otherwise, output ρ_1 and ρ_3 now output $\mathcal{D}_p^{N_1}(\rho_1)$ and $\mathcal{D}_p^{N_3}(\rho_3)$. The expected approximation ratio of magic state rounding corresponding to the resulting noisy states can be derived as

$$\mathbb{E}(\gamma_1') = p^{N_1} + (1 - p^{N_1})\frac{|E|}{2\text{cut}(m^*)} \tag{12}$$

for the Ising Hamiltonian and

$$\begin{aligned}\mathbb{E}(\gamma_3') &= \frac{\mathbb{E}\left[\text{Tr}\left\{\mathcal{M}^{\otimes n_3}(\mathcal{D}_p^{N_3}(\rho_3))H\right\}\right]}{\text{cut}(m*)} \\ &\geq \frac{5}{9}p^{N_3} + (1 - p^{N_3})\frac{|E|}{2\text{cut}(m^*)}\end{aligned} \tag{13}$$

for the QRAC Hamiltonian. Assuming that $p \in (0, 1)$, $N_1 > N_3$, and thus $p^{N_1} > p^{N_3}$, the inequality $\mathbb{E}(\gamma_3') \geq \mathbb{E}(\gamma_1')$ holds only when $\text{cut}(m^*)/|E| \geq 9/10$. This may seem restrictive, but this constraint is to ensure that at one point the lower bound of the expected approximation ratio of the QRAC Hamiltonian exceeds the expected approximation ratio of the Ising Hamiltonian. Because the lower bound is considered for the QRAC Hamiltonian, it is possible for the expected approximation ratio for the QRAC Hamiltonian to exceed that of the Ising Hamiltonian with graphs that do not fulfill $\text{cut}(m^*)/|E| \geq 9/10$.

Considering graphs that satisfy $|E| = \text{cut}(m^*)$, we can analyze the expected approximation ratios of the Ising Hamiltonian and the QRAC Hamiltonian with respect to the number of noisy operations the candidate states have undergone. We consider the ideal case where the QRAC Hamiltonian requires one-third the number of qubits compared to the Ising Hamiltonian, and thus, the QRAC candidate state ρ_3 goes through the depolarizing channel one-third the number of times the Ising Hamiltonian candidate state ρ_1 does. Fig. 5 shows that there exists an N_1, where the lower bound of the expected approximation ratio of the QRAC Hamiltonian exceeds that of the Ising Hamiltonian under depolarizing noise with error probability 1%. The intersection point N_1 decreases as the success probability of each depolarizing noise application declines. Fig. 5 assumes the maximum eigenstate for the Ising Hamiltonian and a state with a higher energy than the maximum cut value for the QRAC Hamiltonian. The difficulty of obtaining the respective states is not taken into consideration, and therefore, Fig. 5 does not necessarily suggest that the Ising Hamiltonian could be more favorable given certain problem instances.

The robustness of the approximation ratio of the QRAC Hamiltonian compared to the Ising Hamiltonian can be explained by the fact that the QRAC Hamiltonian requires fewer qubits to encode the same problem than the Ising Hamiltonian. With fewer qubits, the amount of noisy operations in the PQC is reduced, leading to a candidate state that is less affected by noise. In addition, for Pauli rounding, the robustness is due to the sign of the trace value remaining unaffected under isotropic noise such as depolarizing noise.

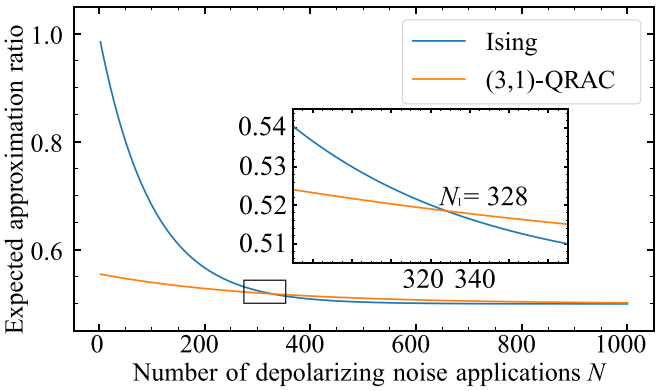

FIGURE 5. Expected approximation ratios of the QRAC Hamiltonian via magic state rounding and the Ising Hamiltonian under depolarizing noise with success probability $p = 0.99$ and the minimum number of depolarizing noise applications required to achieve $\frac{5}{9}p^{N_3} + (1 - p^{N_3})/2 \geq \mathbb{E}(\gamma_1')$. It is assumed that $N_1 = 3N_3$ and $|E|/\text{cut}(m^*) = 1 \geq 9/10$.

IV. CONCLUSION

In this article, we have shown that the mean approximation of QRAO with the QRAC Hamiltonian is more robust to noise compared to the Ising Hamiltonian. We have observed that under fake noise, the mean approximation of the Ising Hamiltonian drops out of the 95% confidence interval, while the mean approximation ratio of the QRAC Hamiltonian does not. In addition, the mean approximation ratio of the QRAC Hamiltonian has been shown to exceed the mean approximation ratio of the Ising Hamiltonian as the problem size increases, even in the absence of noise. We have shown that the mean approximation ratio of the QRAC Hamiltonian is higher in relation to its VQE energy ratio compared to the Ising Hamiltonian. Under the assumption of depolarizing noise, we have explained the robustness of the mean approximation ratio of QRAO by the fact that the sign of the trace values remain unaffected, and have explained the effect of depolarizing noise on the mean approximation ratio of QRAO via magic state rounding by the fact that the candidate state of the QRAC Hamiltonian undergoes less noisy operations in VQE compared to the Ising Hamiltonian due to using fewer qubits. Finally, we have shown that the number of shots required to estimate the correct binary solution with the same level of accuracy is less for the QRAC Hamiltonian, and that the difference increases along with the problem size and the level of noise. These facts indicate that the use of QRAO becomes an evermore realistic option as the problem size increases under noise, because the mean approximation ratio of the QRAC Hamiltonian is expected to exceed the mean

TABLE 1. ***i*th Measurement Result Corresponding to the Pauli Matrix P_j, Where j Is the Node Number**

i	P_1	$\cdots$	P_j	$\cdots$	P_m
1	1	$\cdots$	1	$\cdots$	0
2	0	$\cdots$	1	$\cdots$	1
$\vdots$	$\vdots$	$\vdots$	$\vdots$	$\vdots$	$\vdots$
i	X_{i1}	$\cdots$	X_{ij}	$\cdots$	X_{im}
$\vdots$	$\vdots$	$\vdots$	$\vdots$	$\vdots$	$\vdots$
n	0	$\cdots$	0	$\cdots$	1
$h_1^j = \sum_{i=1}^S X_{ij}$	h_1^1		h_1^j		$h_1^{\lvert V\rvert}$

approximation ratio of the Ising Hamiltonian and requires fewer qubits and shots.

APPENDIX
HOEFFDING–CHERNOFF BOUND FOR PAULI ROUNDING

Given a PQC with optimized parameters, apply the appropriate gate operation to all qubits and perform measurement in the computational basis to estimate the trace values corresponding to the Pauli matrix X, Y, or Z. The appropriate gate operation is the Hadamard gate for the Pauli matrix X, the Hadamard gate, and then the phase gate for the Pauli matrix Y, and for the Pauli matrix Z, no gate operation is necessary.

Let us consider a graph with $|V|$ nodes, where the Pauli matrix corresponding to the jth node is denoted P_j. The measurement results across S shots for the Pauli matrices P_1–P_m are shown in Table 1.

After S shots, we have S measurement results for each node j as $X_{1j}, X_{2j}, \ldots, X_{Sj}$. The trace value is estimated as

$$\begin{aligned}\mathrm{Tr}(P_j\rho) &= 2\left(1 - \frac{\sum_{i=1}^S X_{ij}}{S}\right) - 1 \\ &= 1 - 2\frac{\sum_{i=1}^S X_{ij}}{S} \\ &= 1 - 2\frac{h_1^j}{S}.\end{aligned}$$

Assume that $\Pr[X_{i,j} = 1] = \frac{1}{2} + \varepsilon$, where $\Pr[X_{i,j} = 1]$ is the expectation value of the measurement outcome of $X_{i,j}$, and $\varepsilon > 0$. Note that under this assumption, the trace value is always negative. We estimate the sign of the trace value incorrectly when $h_1^j = \sum_{i=1}^S X_{ij} \leq S/2$, which leads to a positive sign.

Chernoff–Hoeffding Bound: Let $X_{1j}, X_{2j}, \ldots, X_{Sj}$ be independent random variables in $\{0, 1\}$ with $\Pr[X_{i,j} = 1] = p_j$. Let $h_1^j = \sum_{i=1}^S X_{ij}$, $\mu_j = E[h_1^j] = Sp_j$. Then, for any $\lambda > 0$, we have

$$\Pr\left[h_1^j \leq \mu_j - \lambda\right] \leq \exp\left(-\frac{2\lambda^2}{S}\right).$$

By substituting μ with $S(1/2 + \varepsilon)$ and λ with εS, we obtain

$$\begin{aligned}\Pr\left[h_1^j \leq \mu_j - \lambda\right] &= \Pr\left[h_1^j \leq S\left(\frac{1}{2} + \varepsilon\right) - \varepsilon S\right] \\ &= \Pr\left[h_1^j \leq \frac{S}{2}\right] \leq \exp(-2S\varepsilon^2).\end{aligned}$$

Now, we would like to bound the probability of estimating the sign of the trace value incorrectly with δ as

$$\Pr\left[h_1^j \leq \frac{S}{2}\right] \leq \exp\left(-2S\varepsilon^2\right) \leq \delta.$$

From the aforementioned inequality, it follows that

$$S \geq \frac{\ln(1/\delta)}{2\varepsilon^2}.$$

The probability of correctly estimating the sign of the trace values corresponding to all Pauli matrices is given by $(1-\delta)^{|V|}$, which should be close to 1. From Bernoulli's inequality, we have

$$\alpha \leq (1-\delta)^{|V|} \leq \exp(-\delta|V|)$$

from which $\delta \leq -\ln(\alpha)/|V|$ can be derived. Now, we have

$$S = \mathcal{O}\left(\frac{\ln(|V|)}{\varepsilon^2}\right).$$

For m Pauli matrices, the number of shots becomes

$$\mathcal{O}\left(\frac{|V|\ln(|V|)}{\varepsilon^2}\right).$$

In the case where the candidate state ρ is affected by depolarizing noise, the trace value becomes $\mathrm{Tr}(P_j\mathcal{D}_p^N(\rho)) = p^N\mathrm{Tr}(P_j\rho)$. With this in mind, the value of ε can be derived as $\varepsilon = -p^N\mathrm{Tr}(P_j\rho)/2$. Note that the trace value is assumed to be negative.

ACKNOWLEDGMENT

The views expressed are those of the authors and do not reflect the official policy or position of IBM or the IBM Quantum team.

REFERENCES

[1] M. Grotschel and L. Lovász, "Combinatorial optimization," in *Handbook Combinatorics*, vol. 2, Amsterdam, The Netherlands: Elsevier, 1995, pp. 1541–1597. [Online]. Available: https://shop.elsevier.com/books/handbook-of-combinatorics-volume-2/luisa/978-0-444-82351-9

[2] U. Azad, B. K. Behera, E. A. Ahmed, P. K. Panigrahi, and A. Farouk, "Solving vehicle routing problem using quantum approximate optimization algorithm," *IEEE Trans. Intell. Transp. Syst.*, vol. 24, no. 7, pp. 7564–7573, Jul. 2023, doi: 10.1109/TITS.2022.3172241.

[3] K. Kurowski, T. Pecyna, M. Slysz, R. Różycki, G. Waligóra, and J. WóŹglarz, "Application of quantum approximate optimization algorithm to job shop scheduling problem," *Eur. J. Oper. Res.*, vol. 310, no. 2, pp. 518–528, 2023, doi: 10.1016/j.ejor.2023.03.013.

[4] D. J. Egger et al., "Quantum computing for finance: State-of-the-art and future prospects," *IEEE Trans. Quantum Eng.*, vol. 1, 2020, Art. no. 3101724, doi: 10.1109/TQE.2020.3030314.

[5] S. Marsh and J. Wang, "Combinatorial optimization via highly efficient quantum walks," *Phys. Rev. Res.*, vol. 2, 2020, Art. no. 023302, doi: 10.1103/PhysRevResearch.2.023302.

[6] A. Peruzzo et al., "A variational eigenvalue solver on a photonic quantum processor," *Nature Commun.*, vol. 5, no. 1, 2014, Art. no. 4213, doi: 10.1038/ncomms5213.

[7] E. Farhi, J. Goldstone, and S. Gutmann, "A quantum approximate optimization algorithm," 2014, *arXiv:1411.4028*, doi: 10.48550/arXiv.1411.4028.

[8] G. G. Guerreschi and A. Y. Matsuura, "QAOA for max-cut requires hundreds of qubits for quantum speed-up," *Sci. Rep.*, vol. 9, 2019, Art. no. 6903, doi: 10.1038/s41598-019-43176-9.

[9] J. Preskill, "Quantum computing in the NISQ era and beyond," *Quantum*, vol. 2, 2018, Art. no. 79, doi: 10.22331/q-2018-08-06-79.

[10] N. Moll et al., "Quantum optimization using variational algorithms on near-term quantum devices," *Quantum Sci. Technol.*, vol. 3, no. 3, 2018, Art. no. 030503, doi: 10.1088/2058-9565/aab822.

[11] W. Tang, T. Tomesh, M. Suchara, J. Larson, and M. Martonosi, "CutQC: Using small quantum computers for large quantum circuit evaluations," in *Proc. 26th ACM Int. Conf. Archit. Support Program. Lang. Oper. Syst.*, 2021, pp. 473–486, doi: 10.1145/3445814.3446758.

[12] B. Tan, M.-A. Lemonde, S. Thanasilp, J. Tangpanitanon, and D. G. Angelakis, "Qubit-efficient encoding schemes for binary optimisation problems," *Quantum*, vol. 5, 2021, Art. no. 454, doi: 10.22331/q-2021-05-04-454.

[13] H. Yano, Y. Suzuki, K. M. Itoh, R. Raymond, and N. Yamamoto, "Efficient discrete feature encoding for variational quantum classifier," *IEEE Trans. Quantum Eng.*, vol. 2, 2021, Art. no. 3103214, doi: 10.1109/TQE.2021.3103050.

[14] B. Fuller et al., "Approximate solutions of combinatorial problems via quantum relaxations," 2021, *arXiv:2111.03167*, doi: 10.48550/arXiv.2111.03167.

[15] A. Ambainis, A. Nayak, A. Ta-Shma, and U. Vazirani, "Dense quantum coding and quantum finite automata," *J. ACM*, vol. 49, no. 4, pp. 496–511, 2002, doi: 10.1145/581771.581773.

[16] A. S. Holevo, "Bounds for the quantity of information transmitted by a quantum communication channel," *Probl. Peredachi Inf.*, vol. 9, pp. 3–11, 1973.

[17] M. Hayashi, K. Iwama, H. Nishimura, R. Raymond, and S. Yamashita, "(4, 1)-quantum random access coding does not exist—One qubit is not enough to recover one of four bits," *New J. Phys.*, vol. 8, no. 8, 2006, Art. no. 129, doi: 10.1088/1367-2630/8/8/129.

[18] O. Liabøtrø, "Improved classical and quantum random access codes," *Phys. Rev. A*, vol. 95, no. 5, 2017, Art. no. 052315, doi: 10.1103/PhysRevA.95.052315.

[19] T. Imamichi and R. Raymond, "Constructions of quantum random access codes," in *Proc. Asian Quantum Inf. Symp.*, 2018. [Online]. Available: https://research.ibm.com/publications/constructions-of-quantum-random-access-codes

[20] L. Mančinska and S. AL Storgaard, "The geometry of Bloch space in the context of quantum random access codes," *Quantum Inf. Process.*, vol. 21, no. 4, pp. 1–16, 2022, doi: 10.1007/S11128-022-03470-4.

[21] K. Teramoto, R. Raymond, and H. Imai, "The role of entanglement in quantum-relaxation based optimization algorithms," in *Proc. 2023 IEEE Int. Conf. Quantum Comput. Eng.*, 2023, pp. 543–553, doi: 10.1109/QCE57702.2023.00068.

[22] K. Teramoto, R. Raymond, E. Wakakuwa, and H. Imai, "Quantum-relaxation based optimization algorithms: Theoretical extensions," 2023, *arXiv:2302.09481*, doi: 10.48550/arXiv.2302.09481.

[23] R. Kondo, Y. Sato, R. Raymond, and N. Yamamoto, "Recursive quantum relaxation for combinatorial optimization problems," 2024, *arXiv:2403.02045*, doi: 10.48550/arXiv.2403.02045.

[24] A. R. da Silva and B. Marques, "Semidefinite-programming-based optimization of quantum random access codes over noisy channels," *Phys. Rev. A*, vol. 107, 2023, Art. no. 042433, doi: 10.1103/PhysRevA.107.042433.

[25] Qiskit contributors, "Qiskit: An open-source framework for quantum computing," 2023. [Online]. Available: https://github.com/Qiskit/qiskit

[26] R. M. Karp, *Reducibility Among Combinatorial Problems*. Boston, MA, USA: Springer, 1972, pp. 85–103.

[27] M. Benedetti, M. Fiorentini, and M. Lubasch, "Hardware-efficient variational quantum algorithms for time evolution," *Phys. Rev. Res*, vol. 3, Jul. 2021, Art. no. 033083, doi: 10.1103/PhysRevResearch.3.033083.

[28] D. Amaro, C. Modica, M. Rosenkranz, M. Fiorentini, M. Benedetti, and M. Lubasch, "Filtering variational quantum algorithms for combinatorial optimization," *Quantum Sci. Technol.*, vol. 7, no. 1, Feb. 2022, Art. no. 015021, doi: 10.1088/2058-9565/ac3e54.

[29] A. Kandala et al., "Hardware-efficient variational quantum eigensolver for small molecules and quantum magnets," *Nature*, vol. 549, no. 7671, pp. 242–246, 2017, doi: 10.1038/nature23879.

[30] H. C. Watanabe, R. Raymond, Y. -Y. Ohnishi, E. Kaminishi, and M. Sugawara, "Optimizing parametrized quantum circuits with free-axis single-qubit gates," *IEEE Trans. Quantum Eng.*, vol. 4, 2023, Art. no. 3101016, doi: 10.1109/TQE.2023.3286411.

[31] K. Wada et al., "Simulating time evolution with fully optimized single-qubit gates on parametrized quantum circuits," *Phys. Rev. A*, vol. 105, no. 6, 2022, Art. no. 062421, doi: 10.1103/PhysRevA.105.062421.

[32] K. Wada, R. Raymond, Y. Sato, and H. C. Watanabe, "Full optimization of a single-qubit gate on the generalized sequential quantum optimizer," 2022, *arXiv:2209.08535*, doi: 10.48550/arXiv.2209.08535.

[33] K. M. Nakanishi, K. Fujii, and S. Todo, "Sequential minimal optimization for quantum-classical hybrid algorithms," *Phys. Rev. Res.*, vol. 2, no. 4, 2020, Art. no. 043158, doi: 10.1103/PhysRevResearch.2.043158.

[34] M. Ostaszewski, E. Grant, and M. Benedetti, "Structure optimization for parameterized quantum circuits," *Quantum*, vol. 5, 2021, Art. no. 391, doi: 10.22331/q-2021-01-28-391.

[35] T. Tanaka, Y. Suzuki, S. Uno, R. Raymond, T. Onodera, and N. Yamamoto, "Amplitude estimation via maximum likelihood on noisy quantum computer," *Quantum Inf. Process.*, vol. 20, no. 9, 2021, Art. no. 293, doi: 10.1007/s11128-021-03215-9.